WPMST1-PR(18) 21568

DC Moreau et al.

Model-predictive kinetic control for steady state plasma operation scenarios on EAST

Preprint of Paper to be submitted for publication in
Nuclear Fusion

This work has been carried out within the framework of the EUROfusion Consortium and has received funding from the Euratom research and training programme 2014-2018 under grant agreement No 633053. The views and opinions expressed herein do not necessarily reflect those of the European Commission.

Model-predictive kinetic control for steady state plasma operation scenarios on EAST

D. Moreau[1], J.P. Qian[2], Q. Yuan[2], Y. Huang[2], J.F. Artaud[1], S. Ding[2], H. Du[2], M. Li[2], Z. Luo[2], E. Olofsson[3], B. Sammuli[3], S. Wang[4] and E. Witrant[4]

[1] CEA, IRFM, 13108 Saint-Paul-lez-Durance, France
[2] IPP, Chinese Academy of Sciences, Hefei 230031, People's Republic of China
[3] General Atomics, PO Box 85608, San Diego, CA 92186-5608, USA
[4] Université Grenoble-Alpes, CNRS, Grenoble INP, GIPSA-lab, 38000 Grenoble, France

E-mail: didier.moreau@cea.fr

Received xxxxxx
Accepted for publication xxxxxx
Published xxxxxx

Abstract

The paper shows that model-predictive control (MPC) algorithms based on extremely simple linear data-driven models can be used for plasma kinetic control in tokamaks. Such control-oriented models are identified using a two-time-scale approximation, i.e. considering the kinetic plasma dynamics as a singular perturbation of a quasi-static equilibrium, which itself is governed by the flux diffusion equation. This technique takes advantage of the large ratio between the time scales involved in magnetic and kinetic transport, and is applied here to the simultaneous control of the safety factor profile, $q(x)$, and of the poloidal β parameter, β_p, on EAST. The actuators are the LHCD system at 4.6 GHz, the ICRH system, and optionally the plasma surface loop voltage. The models are two-time-scale state-space models identified using datasets obtained from fast, open loop nonlinear METIS simulations, with random actuator modulations. In closed loop, an observer provides, in real time, an estimate of the system states and of the mismatch between measured and predicted outputs, which ensures control robustness to model errors. Based on this information, the controller predicts the behavior of the system over a given time horizon and computes the optimum actuation, taking the actuator constraints into account. For plasma parameters typical of the high-β_p steady state operation scenarios on EAST, nonlinear closed loop simulations show that various $q(x)$ profiles and β_p waveforms can be tracked in about 2.5 s and 0.2 s, respectively.

Keywords: tokamaks, steady state operation scenarios, plasma control, profile control, model-predictive control, plasma simulation, plasma heating and current drive.

1. Introduction

Simultaneous magnetic and kinetic plasma control based on extremely simple linear data-driven models identified using a two-time-scale approximation has been developed in recent years [1]. Ideally, first-principles plasma transport models could be preferred as they should have a universal domain of validity, but despite their increasing complexity, they still depend on many uncertain parameters and their accuracy cannot be widely assessed, even in their linearized version for real-time control applications. So the idea here is to free oneself from the complexity of such models and to reduce the control computational cost, at the expense of a more restricted applicability (e.g. to a given device, actuator set and operation scenario). In the so-called ARTAEMIS two-time-scale models and in the associated control

algorithms, the fast component of the kinetic plasma dynamics, including in particular momentum and thermal diffusion, is considered as a singular perturbation of a quasi-static equilibrium, which itself is governed on the resistive timescale by the flux diffusion equation. The system identification problem is thus made tractable by the partial decoupling of the slow and fast dynamics. Combined with linear-quadratic optimal control theory, the effectiveness of this approach to simultaneously control the plasma poloidal flux profile, $\psi(x)$, and the normalized pressure parameter, β_N, in non-inductive, high-β_N discharges was demonstrated experimentally on the DIII-D tokamak [2]. Using the same approach, simultaneous control of the safety factor profile, $q(x)$, and plasma pressure was also achieved in closed loop nonlinear plasma transport simulations [3]. However, in such simulations the desired steady state q-profiles were obtained either much too slowly, or after a large undershoot of the safety factor in the plasma core with respect to its target value and a damped oscillation. A non-monotonic approach of the q-profile to its target profile is not desirable, as it may lead to MHD instabilities during the build up of the plasma equilibrium.

In view of upcoming profile control experiments on EAST, recent work was therefore dedicated to the development of new algorithms combining, for the first time, the simplicity of the ARTAEMIS models based on singular perturbation theory with model-predictive control (MPC) techniques [4]. For the applications presented in this paper, the control actuators are: off-axis lower hybrid current drive (LHCD) power at 4.6 GHz, central ion cyclotron resonance heating (ICRH) power at 33 MHz and, optionally, the plasma surface loop voltage, V_{surf}. The goal is to control the q-profile and the poloidal β parameter, β_p, in a high-β_p fully non-inductive operation scenario. It was already shown earlier for several other tokamaks [1-3] that two-time-scale models can satisfactorily approximate the coupled response of the magnetic and kinetic plasma parameters and profiles to relatively large random variations of the heating and current drive actuators available on a particular device, in a given operation scenario. Such models have therefore been easily identified for EAST by applying the ARTAEMIS system identification procedure [1] to simulated data obtained from the nonlinear METIS plasma simulator [5], with random open loop actuator modulations. A new ARTAEMIS MPC controller has been synthesized and coupled with the METIS code for non-linear closed loop control simulations. Then, in order to tune the adjustable controller parameters, extensive simulations have been performed with various target q-profiles, and with different β_p target waveforms. The validation of the new MPC algorithm from these results is the main objective of this paper.

The description of the scenario chosen for the open loop METIS simulations and of the linear ARTAEMIS model used in the MPC controller for the closed loop simulations will be the subject of the next section. Then, in section 3, the details of the MPC algorithm will be described. Finally, the results of control simulations where the $q(x)$ and β_p targets have been varied will be presented in sections 4 and 5. Examples with flat or monotonic q-profiles, and with different β_p waveforms will be discussed.

2. METIS simulations and ARTAEMIS semi-empirical state space models

The ARTAEMIS model used in the present work describes the coupled time evolution of $\psi(x,t) = \Psi(x,t) - \Psi_{\mathrm{b}}(t)$ where x is a normalized radial coordinate defined below, $\Psi(x,t)$ is the poloidal magnetic flux profile in Webers and $\Psi_{\mathrm{b}}(t)$ its value at the plasma boundary, of $\bar{\iota}(x,t) = 1/q(x,t)$, and of the slow (quasi-static) and fast components of $\beta_p(t)$ ($\beta_{p,\mathrm{S}}$ and $\beta_{p,\mathrm{F}}$, respectively), with $\beta_p(t) = \beta_{p,\mathrm{S}}(t) + \beta_{p,\mathrm{F}}(t)$. Details concerning this approximation and the identification of a two-time-scale plasma response model from experimental or simulated data are given in references [1-3]. The general structure of the model is postulated from the projection onto radial basis functions (cubic splines) of a set of coupled plasma response equations that only depend on x and t, and which stem from the linearized flux-averaged plasma transport equations. A lumped-parameter, linear time-invariant, control-oriented model is thus obtained, in which all distributed variables and unknown operators reduce to finite dimension vectors and matrices. It combines a slow dynamic model, which couples ψ and β_p,

$$\dot{X}_S(t) = A_S \cdot X_S(t) + B_S \cdot U_S(t) \tag{1}$$

$$\psi(t) = C_{\psi} \cdot X_S(t) \tag{2}$$

$$\beta_{p,S}(t) = C_S \cdot X_S(t) + D_S \cdot U_S(t) \tag{3}$$

and a fast dynamic model,

$$\dot{X}_F(t) = A_F \cdot X_F(t) + B_F \cdot U_F(t) \tag{4}$$

$$\beta_{p,F}(t) = C_{\beta} \cdot X_F(t) \tag{5}$$

where A_{S} and A_{F} are regular matrices with negative eigenvalues. The vector U, containing the actuator inputs, is also split into a slow and a fast component ($U = U_{\mathrm{S}} + U_{\mathrm{F}}$). The q-profile is controlled through its inverse,

$$\bar{\iota}(x,t) = \iota(x,t)/(2\pi) = 1/q(x,t) = -\left[\partial\psi(x,t)/\partial x\right]\cdot\left[\partial\Phi(x,t)/\partial x\right]^{-1} \tag{6}$$

where $\Phi(x, t)$ is the toroidal magnetic flux in Webers, $\Phi_{\max} = \Phi(x=1)$ is its value at the plasma boundary, which is assumed

constant, and $x=(\Phi/\Phi_{max})^{1/2}$. After linearization around the reference plasma equilibrium and projection of $\psi(x,t)$ and of $\bar{\iota}(x,t)$ on the radial basis functions, the vector $\bar{\iota}(t)$ can therefore be related to the vector $\psi(t)$ through a linear output equation,

$$\bar{\iota}(t) = \Gamma_\iota \cdot \psi(t) = C_\iota \cdot X_S(t) \quad (7)$$

In order to identify the various matrices in the ARTAEMIS model corresponding to the selected operation scenario on EAST, a large number of nonlinear simulations were performed using the METIS plasma simulator [5] tuned for the reference discharge #62946, until a fair agreement with experimental data and interpretative TRANSP simulation results was obtained. This procedure was previously used for DIII-D and is described in reference [3]. The resulting datasets were then used in the ARTAEMIS system identification algorithm [1-3].

The reference scenario around which the linear response model was identified was a steady state, fully non-inductive single-null H-mode discharge, at a toroidal magnetic field, B_T = 2.5 T, central electron density, $n_{e0} \approx 3.5\text{x}10^{19}$ m^{-3}, and plasma current, I_p = 0.42 MA. The discharge had been obtained using LHCD (0.6 MW at 2.45 GHz and 2 MW at 4.6 GHz), 0.32 MW of ICRH at 33 MHz and 0.3 MW of ECRH (electron cyclotron resonance heating) at 140 GHz. The transition to H-mode occurred at 3.1 s with an H-factor, $H_{98(y,2)} \sim 1.1$. The steady state poloidal β and internal inductance parameters were β_p = 1.3 and l_i = 1.2, respectively, and the q-profile exhibited a small negative shear in the plasma core, with a minimum q around 1.5 and $q_0 \sim 2$ on axis. The plasma parameter profiles are obtained from EFIT magnetic equilibrium reconstructions, which are available in real-time using magnetic and kinetic measurements, including interfero-polarimetry data from the POINT diagnostic. Two important parameters characterizing the identified models are the largest (negative) eigenvalues of A_S and A_F, found as -1.19 and -24.8 s^{-1}, which correspond to time constants τ_S = 0.840 s and τ_F = 0.040 s for the resistive (slow model) and thermal (fast model) diffusion timescales, respectively.

3. State observer, model errors and MPC controller design

In order to make the controller robust to model uncertainties, the identified model is augmented with an output disturbance model, which is used to estimate the mismatch between measured and predicted outputs in steady state [6]. Thus, at each time step, an observer provides a new estimate of the evolving system states and of the steady state errors, and the controller uses the augmented model with constant errors to predict the behavior of the system over a future time horizon. In its continuous time version[1], the augmented model reads:

$$\dot{X}_S(t) = A_S \cdot X_S(t) + B_S \cdot U_S(t) \quad (8)$$

$$\dot{X}_F(t) = A_F \cdot X_F(t) + B_F \cdot U_F(t) \quad (9)$$

$$\dot{d}_\iota(t) = 0 \quad (10)$$

$$\dot{d}_\beta(t) = 0 \quad (11)$$

$$\bar{\iota}(t) = C_\iota \cdot X_S(t) + d_\iota(t) \quad (12)$$

$$\beta_p(t) = C_S \cdot X_S(t) + D_S \cdot U_S(t) + C_\beta \cdot X_F(t) + d_\beta(t) \quad (13)$$

where $d_\iota(t)$ and $d_\beta(t)$ are disturbance vectors representing the errors on $\bar{\iota}(t)$ and $\beta_p(t)$, respectively, $U_S(t)$ is obtained through a simple low-pass filter and $U_F(t) = U(t) - U_S(t)$. The filter cutoff frequency, $f_{filt} = 1/\tau_{filt}$, is chosen during the model identification and is such that $\tau_F << \tau_{filt} << \tau_S$. The filter states that allow $U_S(t)$ and $U_F(t)$ to be computed in the observer at time t are transmitted to the controller with the estimated system states and disturbances and with the real-time measurements of the controlled variables, $\bar{\iota}_m(t)$ and $\beta_{p,m}(t)$.

The state and disturbance estimator is a classical Luenberger observer based on the augmented system above, and is designed as follows:

$$\dot{\hat{X}}_S(t) = A_S \cdot \hat{X}_S(t) + B_S \cdot U_S(t) + K_{11} \cdot \left(-\bar{\iota}_m(t) + C_\iota \cdot \hat{X}_S(t) + \hat{d}_\iota(t)\right) + K_{12} \cdot \left(-\beta_{p,m}(t) + C_S \cdot \hat{X}_S(t) + D_S \cdot U_S(t) + C_\beta \cdot \hat{X}_F(t) + \hat{d}_\beta(t)\right) \quad (14)$$

$$\dot{\hat{X}}_F(t) = A_F \cdot \hat{X}_F(t) + B_F \cdot U_F(t) + K_{21} \cdot \left(-\bar{\iota}_m(t) + C_\iota \cdot \hat{X}_S(t) + \hat{d}_\iota(t)\right) + K_{22} \cdot \left(-\beta_{p,m}(t) + C_S \cdot \hat{X}_S(t) + D_S \cdot U_S(t) + C_\beta \cdot \hat{X}_F(t) + \hat{d}_\beta(t)\right) \quad (15)$$

$$\begin{bmatrix} \dot{\hat{d}}_\iota(t) \\ \dot{\hat{d}}_\beta(t) \end{bmatrix} = K_{31} \cdot \left(-\bar{\iota}_m(t) + C_\iota \cdot \hat{X}_S(t) + \hat{d}_\iota(t)\right) + K_{32} \cdot \left(-\beta_{p,m}(t) + C_S \cdot \hat{X}_S(t) + D_S \cdot U_S(t) + C_\beta \cdot \hat{X}_F(t) + \hat{d}_\beta(t)\right) \quad (16)$$

where symbols with a hat represent the estimates of the system states and disturbances, and the $K_{i,j}$ matrices are chosen so that $[K_{31}\ K_{32}]$ is non singular, and the estimator is stable and converges rapidly. The observer then tracks the

[1] For notation convenience, the systems presented in this paper are continuous-time systems. Their conversion to discrete-time systems is straightforward and was carried out for the controller implementation on the METIS simulator and on EAST.

measurements without steady state error ($\dot{\hat{d}}_{\iota} = \dot{\hat{d}}_{\beta} = 0$). In addition, by definition, the fast variables U_F, X_F and $\beta_{p,F}$ vanish in steady state, and the observer therefore satisfies (the ∞ symbol indicates steady state):

$$\hat{X}_{S,\infty} = -A_S^{-1} \cdot B_S \cdot U_\infty \tag{17}$$

and

$$K_S \cdot U_\infty = \begin{bmatrix} \overline{\iota}_{m,\infty} - \hat{d}_{\iota,\infty} \\ \beta_{p,m,\infty} - \hat{d}_{\beta,\infty} \end{bmatrix} \tag{18}$$

with

$$K_S = \begin{bmatrix} -C_{\iota} \cdot A_S^{-1} \cdot B_S \\ -C_S \cdot A_S^{-1} \cdot B_S + D_S \end{bmatrix} \tag{19}$$

The controller objective is to make $\overline{\iota}_{m,\infty}$ and $\beta_{p,m,\infty}$ equal to $\overline{\iota}_{target}$ and $\beta_{p,target}$, respectively (offset-free control), or as close as possible if the dimension of the image space of K_S spun by the actuators is smaller than the number of controlled variables. In order to avoid combinations of actuators which would lead to unnecessary actuation cost, a singular decomposition of K_S will be used and the allowed actuator space will be limited to the first n_{svd} singular vectors of K_S, i.e. $U = T_{svd} \cdot V$, where n_{svd} (the dimension of V) is a free parameter. At each time step, the MPC algorithm then solves a quadratic programming (QP) problem using the predicted evolution of the augmented system over a time horizon, τ_H, which is chosen of the order of τ_S, or smaller. A long time horizon may not be meaningful because the prediction is made with the assumption that the estimated error at time t will be constant between t and $t + \tau_H$. The QP problem to be solved at time t reads as follows:

For $t \le t' \le t + \tau_H$, find $V(t')$ that minimizes

$$\begin{aligned} I_H(t) = & \int_t^{t+\tau_H} dt' \left\{ \int_0^1 dx\, \mu(x)^2 \left[\overline{\iota}(x,t') - \overline{\iota}_{\text{target}}(x) \right]^2 \right\} \\ & + \int_t^{t+\tau_H} dt' \left\{ \lambda_{kin}^2 \left[\beta_p(t') - \beta_{p,\text{target}} \right]^2 \right\} \\ & + \int_t^{t+\tau_H} dt' \left\{ \lambda_{fast}^2 \cdot X_F(t')^2 + R \cdot \left[U(t') - U_\infty \right]^2 \right\} \end{aligned} \tag{20}$$

with $U(t') = T_{svd} \cdot V(t')$, subject to the actuator constraints $L \cdot U(t') \le M$, while $X_S(t')$, $X_F(t')$, $\overline{\iota}(t')$, $\beta_p(t')$, $d_{\iota}(t')$ and $d_{\beta}(t')$ evolve according to the augmented system, with the initial conditions:

$X_S(t'=t) = \hat{X}_S(t)$, $X_F(t'=t) = \hat{X}_F(t)$, $d_{\iota}(t'=t) = \hat{d}_{\iota}(t)$ and $d_{\beta}(t'=t) = \hat{d}_{\beta}(t)$. In order to keep the computation time small, $V(t')$ is constrained as piecewise constant functions with only n_{nodes} independent unknowns equidistributed over the horizon τ_H. The free parameters $\mu(x)$ and λ_{kin} are weights given to the various variables to be controlled, λ_{fast} is a weight given to the fast model states that can moderate the kinetic control response time, and R is a positive matrix that can moderate the controller actuation effort. Once the QP problem has been solved, the first sample $U(t'=t)$ is used for the actuator commands at time t. The minimized cost function penalizes, with appropriate weights, the deviations of the predicted controlled outputs from their targets, as well as the actuator power if $R \neq 0$. Another way to moderate the actuation effort and avoid overshoots and oscillations is to reshape the targets waveforms in $I_H(t)$ so that they approach the set-points exponentially from their current values, $\overline{\iota}_m(t)$ and $\beta_{p,m}(t)$, with a time constant, τ_{target}, of the order of τ_S [4].

4. Simulations of the safety factor and β_p control on EAST

To illustrate and validate the new ARTAEMIS MPC control algorithm presented above, we shall now describe the results of nonlinear closed loop simulations in a high-β_p non-inductive scenario on EAST. The simulations were performed by inserting the METIS code at the output of the controller in a MATLAB®/Simulink model, and feeding the appropriate METIS outputs back into the controller. Many plasma parameters or profiles such as the plasma shape, B_T, n_{e0}, etc., will be assumed independent of the actuators and were fixed external inputs to the code, together with all the chosen METIS options for modeling the various physical phenomena. The time evolution of these parameters and profiles was based on the actual experimental data from shot #62946 until t = 3.2 s when control was switched-on. They were held constant afterwards. Also, constant feedforward LHCD at 2.45 GHz (0.6 MW) and ECRH (0.3 MW) were used in all simulations, as in the reference shot. For $t \ge 3.2$ s, at each time step with a sampling time of 20 ms, the 4.6 GHz LHCD and 33 MHz ICRH actuator powers were prescribed by the controller and the evolution of all the plasma parameters and profiles that depend on the injected power (e.g. I_p, V_{surf}, l_i, β_p, $\Psi(x, t)$, $q(x, t)$, temperature profiles, etc.) was simulated. The controller filter cutoff and the number of nodes during the horizon were chosen as τ_{filt} = 0.2s and n_{nodes} = 2, respectively, and have been unchanged for all the simulations presented below. The constraint matrices L and M were defined as to bound the 4.6 GHz LHCD power to $0 \le P_{LHCD} \le 3$ MW and the ICRH power to $0 \le P_{ICRH} \le 1.5$ MW.

All the simulations presented in this paper were performed in the current control mode in which the surface loop voltage is used to track a given I_p waveform, as in the reference discharge. When the plasma state is relatively close to the required equilibrium, the controller can also be used in the voltage control mode where V_{surf} can either be fixed to zero for non-inductive operation, or be used as a profile control actuator in addition to LHCD and ICRH. The plasma current is then allowed to float within some bounds, but it is regulated through the control of the safety factor across the entire plasma cross-section ($0 \le x \le 0.9$).

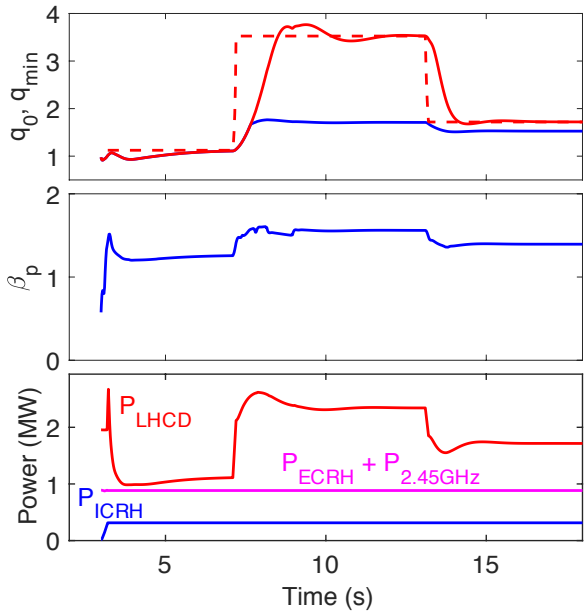

Figure 1. *q_0 control with LHCD only. Top: $q_0(t)$ (red solid), $q_{0,target}(t)$ (red dashed) and $q_{min}(t)$ (blue) vs time. Middle: β_p vs time (not controlled). Bottom: 4.6 GHz LHCD actuator power (red) and feedforward powers: ICRH (blue) and ECRH plus 2.45GHz LHCD (magenta).*

4.1 Control of the safety factor with LHCD

The simplest test of the controller is to track a given target value of the safety factor at a given normalized radius, using the 4.6 GHz LHCD actuator only. In this case, offset-free MPC is possible with the controller synthesis described in section 3, as was proved in reference [6] when the number of controlled variables is equal to the number of actuators or smaller. At constant plasma current, the most sensitive area to control $q(x)$ is the plasma core, and in particular the magnetic axis. An example is displayed on Fig.1 where the controller was requested to track subsequently three different target values of $q_0 = q(x=0)$, namely $q_{0,target}$ = 1.1, 3.5 and 1.7. The ICRH power was fixed (0.32 MW), and the controller parameters were chosen as $n_{svd} = 1$ (since there is only one actuator), $R = 0$, $\tau_{target} = \tau_H = \tau_S = 0.84$ s. The weight function, $\mu(x)$, was replaced by the Dirac distribution, $\delta(0)=1$ and $\delta(x\neq0)=0$, and $\lambda_{kin} = \lambda_{fast} = 0$ since there is no kinetic control. Fig.1 also shows the time evolution of the minimum $q(x)$ across the plasma and of β_p. The tracking of the different q_0 targets in the time intervals 3.2s $\le t \le$ 7.1s, 7.2s $\le t \le$ 13.1s and 13.2s $\le t \le$ 18s, respectively, is performed in about 2 to 3 s, i.e. a few resistive times, and without steady state offset. The time evolution of the minimum q-value (top frame, blue trace) indicates that the second q_0 target yields a q-profile with a strong negative shear in the plasma core (minimum value q_{min} = 1.7). The bottom frame shows the evolution of the 4.6 GHz LHCD power requested by the controller and of the constant feedforward ICRH, ECRH and 2.45 GHz LH powers.

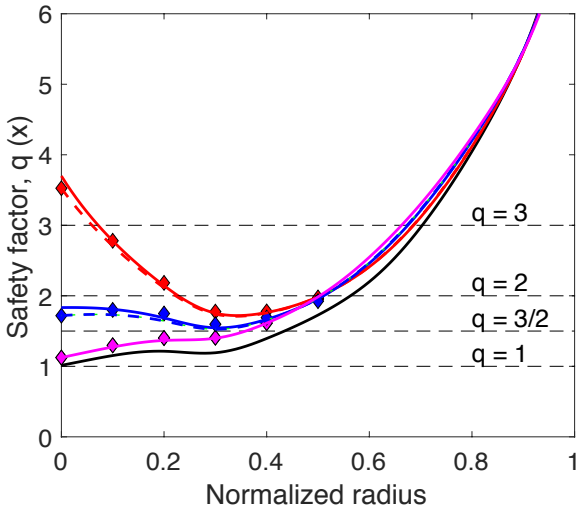

Figure 2. *$q(x)$ control with $\mu(x)=1$ for $0 \le x \le 0.5$ and with LHCD only. Achieved $q(x)$ at t=3.2s (black), 7.1s (magenta), 13.1s (red solid), and 18s (blue solid). Target profiles are constant during these intervals (diamond symbols). Dashed lines are profiles achieved with q_0 control only (see Fig.1).*

Distributed control of the q-profile can also be performed using piecewise linear weight functions, $\mu(x)$, defined and equal to 0 or 1 at the radial knots of the basis functions, x_k = 0, 0.1, 0.2, …1. In this case, genuine offset-free control cannot be sought but the controller is designed to achieve a least-square minimization of the radially integrated error signals, as can be seen in the definition of the cost function $I_H(t)$. When I_p is fixed, there is no need to control the safety factor in the outer edge of the plasma. However, it is important to select target profiles that are accessible (or nearly accessible) with the available actuators so that the least-square approach is meaningful. In practice such profiles can be obtained offline from open loop simulations using a plasma simulator such as METIS, or using more sophisticated models. For comparison with the previous case, an example is shown in Fig.2 with three different q-profile

targets having the same values as in Fig.1 but with $\mu(x_k) = 1$ for $0 \le x_k \le 0.5$. The target q-profiles were chosen from METIS simulations with powers different from the reference discharge, and are represented by diamond symbols. The other controller parameters, constraints and feedforward powers were the same as for the previous example. The q-profile at the start of control (t = 3.2s) is shown by the black curve on Fig.2. The first target profile was a monotonic profile with $q_0 = q_{\min} = 1.1$ (represented by magenta diamonds), and was tracked for 3.2s $\le t \le$ 7.1s. The profile represented by the magenta line is the achieved q-profile at t = 7.1s, in steady state. It is achieved with no offset, showing that the chosen target is consistent with the family of plasma equilibriums that can be obtained in this scenario with the available feedback and feedforward actuators. At this time, the target profile is suddenly changed into the negative shear safety factor profile with $q_0 = 3.5$ and $q_{\min} = 1.7$ (red diamonds) until t = 13.1s when the target profile is changed again to the weak shear profile with $q_0 = 1.7$ and $q_{\min} = 1.6$ (blue diamonds). The controller behaves very similarly as in Fig.1, but with a small steady state offset on axis, which is compensated by a better tracking of the target profile up to x=0.5 (including the region of minimum q). The solid red and blue lines are the profiles achieved at t = 13.1 s and t = 18s, respectively. For comparison, the dashed lines on Fig.2 represent the profiles achieved in the previous case, i.e. with q_0 control only, at the same times.

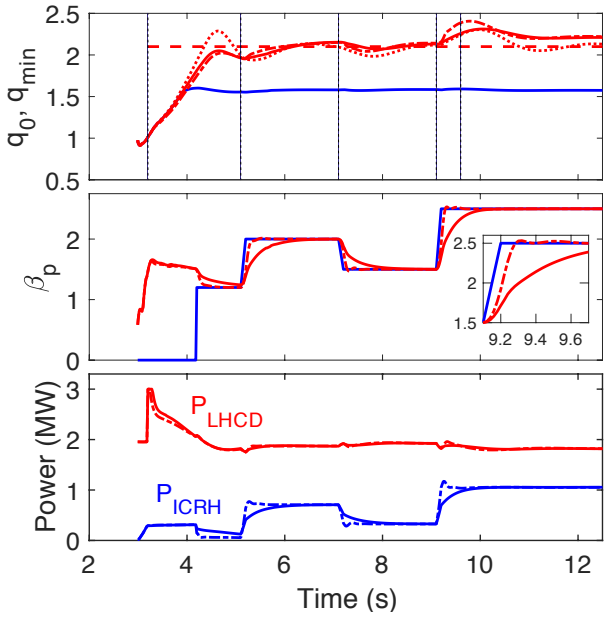

Figure 3. *Distributed q(x) control and slow β_p control with LHCD and ICRH. Top: $q_0(t)$ (red solid, the dotted red line is from discrete q_0 and β_p control for comparison), $q_{0,target}(t)$ (red dashed) and $q_{min}(t)$ (blue). Middle: $\beta_p(t)$ (red solid) and $\beta_{p,target}(t)$ (blue). Bottom: LHCD (red) and ICRH (blue) actuator powers. β_p control starts at 4.2s while q(x) control starts at 3.2s. The dash-dot lines are from fast β_p control.*

4.2 Simultaneous control of q(x) and β_p with LHCD and ICRH based on the slow ARTAEMIS model

The two-time-scale ARTAEMIS models describe the fast kinetic dynamics of the plasma as a singular perturbation of a quasi-static equilibrium, which is slowly evolving due to the coupling between the kinetic and the magnetic plasma parameters. Local dependences of the plasma transport coefficients on the safety factor profile or on the magnetic shear are well-known examples of the various causes that lead to such coupled dynamics. When attempting to control simultaneously the safety factor profile and some other kinetic plasma parameters (e.g. β_p or β_N), it may be unnecessary or even sometimes undesirable to request changes of such parameters on a timescale that is too short compared to the resistive evolution of the plasma equilibrium. Restricting the model to the zero-order equations in the singular perturbation analysis, i.e. to the slow model, will result in a slower kinetic control, but it may preserve a quasi-static equilibrium relationship between various plasma parameters during the transient evolution from an initial plasma state to the desired high performance steady state. Among other advantages of neglecting the fast model altogether is that it reduces the dimension of the QP problem to be solved and therefore alleviates the real-time computations at each time step. This would be mostly beneficial for the control of kinetic profiles (e.g. temperature, rotation) rather than of a scalar like β_p.

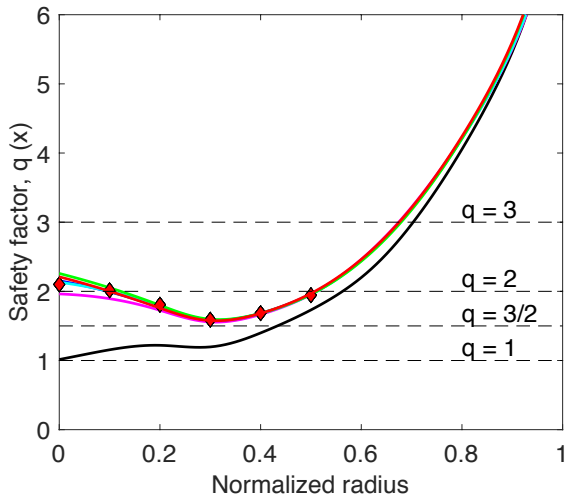

Figure 4. *Combined distributed q(x) control and slow β_p control with LHCD and ICRH. Achieved q(x) at t=3.2s (black), 5.1s (magenta), 7.1s (blue), 9.1s (cyan), 9.6 (green) and 12.5s (red). These times are shown on Fig.3 by vertical lines. The target q-profile is constant (diamond symbols) and $\mu(x)$=1 for $0 \le x \le 0.5$. β_p control starts at 4.2s while q(x) control starts at 3.2s.*

An example of the simultaneous control of $q(x)$ and β_p on the slow (resistive) timescale, with LHCD and ICRH, is

depicted on Fig.3 and Fig.4. Four different β_p targets were tracked, $\beta_{p,target}$ = 1.2 from t = 4.2s to t = 5.1s, and $\beta_{p,target}$ = 2, 1.5 and 2.5 for 5.2s ≤ t ≤ 7.1s, 7.2s ≤ t ≤ 9.1s and t ≥ 9.2s, respectively. The q-profile is controlled from t = 3.2s and between x = 0 and x = 0.5 ($\mu(x)$ = 1 for 0 ≤ x ≤ 0.5), and the target q-profile is constant while β_p changes. As before, R = 0 and λ_{fast} = 0 (no fast model), but here $\tau_{target} = \tau_H = \tau_S/2$ = 0.42 s and, for t ≥ 4.2s, n_{svd} = 2 and λ_{kin} = 1 (normalized variables are used in the controller). Fig.3 shows the time evolution of q_0, q_{min}, the target and achieved β_p, and the actuator powers. Fig.4 shows the achieved q-profiles at the start of the control phase and at the end of each constant $\beta_{p,target}$ phases, and the target q-profile. An additional profile is shown at t = 9.6s, which corresponds to the largest transient q_0 offset during the transition to the β_p = 2.5 plasma equilibrium (Fig.3). As mentioned before, steady state offsets generally remain with distributed q-profile control due to the insufficient number of actuators. The q-profile offset is mostly apparent near the magnetic axis where the safety factor is highly sensitive to any perturbation. The steady state q_0 offset disappears when only q_0 and β_p are controlled, as shown by the dotted red trace on Fig.3 (top frame) at t = 7.1s, 9.1s and 12.5s.

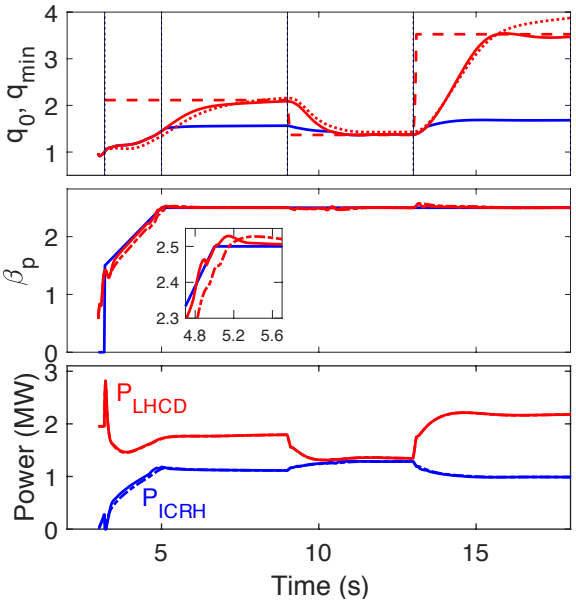

Figure 5. *Combined q_0 and fast β_p control from t=3.2s with LHCD and ICRH. Top: q_0(t) (red solid, the dotted red line is from distributed q(x) and fast β_p control for comparison), $q_{0,target}$(t) (red dashed) and q_{min}(t) (blue). Middle: β_p(t) (red solid) and $\beta_{p,target}$(t) (blue). Bottom: LHCD (red) and ICRH (blue) powers. The dash-dot lines are from slow β_p control.*

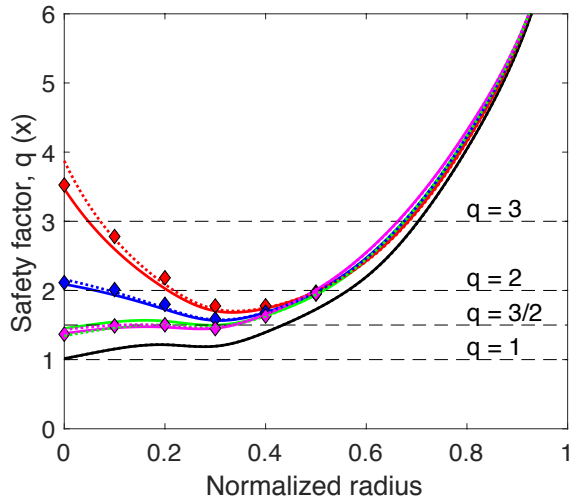

Figure 6. *Combined q_0 and fast β_p control with LHCD and ICRH. Achieved profiles at t=3.2s (black), 5s (green), 9s (blue), 13s (magenta), and 18s (red). These times are shown on Fig.5 by vertical lines. The dotted lines are from distributed q(x) and fast β_p control for comparison. The q(x) targets (diamond symbols) are held constant during these time intervals. β_p and q(x) control starts at 3.2s.*

4.3 Faster control of β_p using the two-time-scale ARTAEMIS model

To illustrate the combination of MPC with singularly perturbed dynamic models with two time scales, we describe now the simultaneous control of $q(x)$ and β_p including the first-order perturbation of the identified model, i.e. the fast model and states, in the control algorithm. The effect can be seen on Fig.3 where we have superimposed the result of the fast β_p control using λ_{fast} = 1.5 (dash-dot lines). Another example shown on Fig.5 and Fig.6 combines a β_p ramp request for 3.2s ≤ t ≤ 5s up to β_p = 2.5, either with fast control (λ_{fast} = 3, solid lines) or without (dashed lines), followed by the tracking of three different q-profiles at constant β_p, either with distributed $q(x)$ control (dotted lines) or with discrete q_0 control (solid lines). Here $\tau_H = \tau_S$ = 0.84 s, $\tau_{target} = 2\tau_S$ = 1.68s, n_{svd} = 2 and λ_{kin} = 1. The first q-profile target has q_0 = 2.1 and q_{min} = 1.6, the second one has $q_0 = q_{min}$ = 1.4, and the last one has q_0 = 3.5 and q_{min} = 1.7 with a large negative magnetic shear over a broad region of the plasma (x ≤ 0.32). Note that increasing τ_{target} results in a smooth approach to the various q_0 targets (Fig.5).

Finally, on Fig.7 and Fig.8, combinations of four different values of $\beta_{p,target}$ = 1.5, 2, 2.5 and 3, and three different q-profiles are tracked successively using the same distributed $q(x)$ control as before, with $\tau_H = \tau_S$ = 0.84 s, $\tau_{target} = 2\tau_S$ = 1.68s, n_{svd} = 2 and λ_{kin} = 1. Again, one can compare the results with fast control (λ_{fast} = 3, solid lines) and without (dashed lines). The q-profile targets are all reached in about

2.5 s (≈ 3 resistive times) and the actuators adjust to reach the various β_p targets within about 0.2s (≈ $5\tau_E$) with fast control and 0.4-0.5s (≥ $10\tau_E$ or $0.5\tau_S$) with slow control, while restoring the desired q-profile shape after each large β_p perturbation.

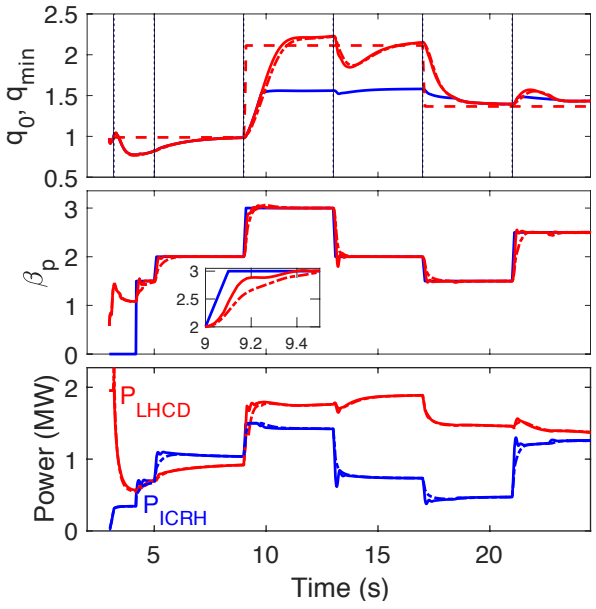

Figure 7. *Distributed q(x) and fast β_p control with LHCD and ICRH. Top: $q_0(t)$ (red solid), $q_{0,target}(t)$ (red dashed) and $q_{min}(t)$ (blue). Middle: $\beta_p(t)$ (red solid) and $\beta_{p,target}(t)$ (blue). Bottom: LHCD (red) and ICRH (blue) actuator powers. The dash-dot lines are from slow β_p control.*

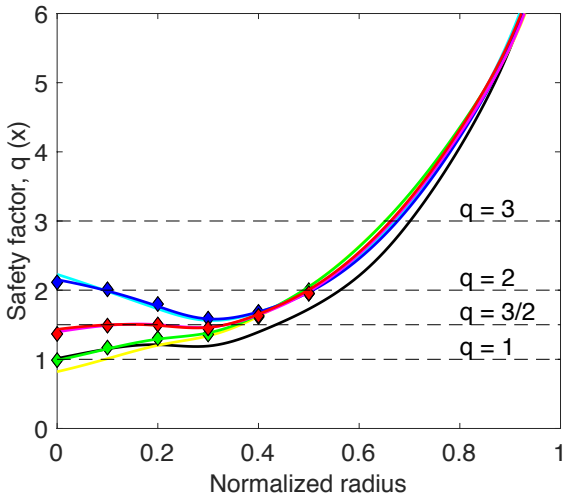

Figure 8. *Distributed q(x) and fast β_p control with LHCD and ICRH. Achieved q(x) at t=3.2s (black), 5s (yellow), 9s (green), 13s (cyan), 17s (blue), 21s (magenta), 25s (red). These times are shown on Fig.7 by vertical lines. β_p and q-profile targets (diamond symbols) are held constant during these time intervals. $\mu(x)=1$ for $0 \le x \le 0.5$.*

5. Conclusions and perspectives

For complex systems with multiple time scales such as tokamak plasmas, model-predictive control can be combined with singular perturbation theory to synthesize fast controllers based on extremely simple, data-driven, two-time-scale models. This has been demonstrated for the first time in this work through extensive non-linear simulations for the high β_p operation scenario in the EAST tokamak. Simultaneous control of the plasma safety factor profile and of the poloidal β parameter was achieved using LHCD and ICRH actuators. The offset-free MPC algorithm used here includes a real-time estimation of the model errors. This yields a more accurate and more robust performance than the linear-quadratic optimal control used previously with similar models (see Ref. [3]). Incorporating feedforward control, better robustness to perturbations, and possibly real-time adaptive model identification can lead to further improvements. The technique should now be assessed experimentally on EAST. It can also be easily extended to the simultaneous control of the q-profile and other kinetic variables or profiles (e.g. β_N, ion or electron temperature, plasma rotation, or fusion reaction rate in burning plasmas).

Acknowledgements

This work has been carried out within the framework of the EUROfusion Consortium and has received funding from the Euratom research and training programme 2014-2018 under grant agreement No 633053. The views and opinions expressed herein do not necessarily reflect those of the European Commission.

References

[1] Moreau D., Mazon D., Walker, M.L. et al., 2015 *Nucl. Fusion* **51** 063009
[2] Moreau D., Walker M.L., Ferron J.R. et al., 2013 *Nucl. Fusion* **53** 063020
[3] Moreau D., Artaud J.F., Ferron J.R. et al., 2015 *Nucl. Fusion* **55** 063011
[4] Maciejowski J.M., *Predictive Control with Constraints*, Pearson Education Limited, Harlow, England (2002)
[5] Artaud J.F., Imbeaux F., Garcia J. et al., 2018 *Nucl. Fusion* **58** 105001
[6] Borrelli F., Morari M., "*Offset free model predictive control*", 46th IEEE Conference on Decision and Control (Proc. IEEE Conf. New Orleans, USA, 2007), WePI19.2